

# The Widely Linear Complex Ornstein-Uhlenbeck Process with Application to Polar Motion

Adam M. Sykulski, *Member, IEEE*, Sofia C. Olhede, *Member, IEEE*, and Hanna M. Sykulska-Lawrence

**Abstract**—Complex-valued and widely linear modelling of time series signals are widespread and found in many applications. However, existing models and analysis techniques are usually restricted to signals observed in discrete time. In this paper we introduce a widely linear version of the complex Ornstein-Uhlenbeck (OU) process. This is a continuous-time process which generalises the standard complex-valued OU process such that signals generated from the process contain elliptical oscillations, as opposed to circular oscillations, when viewed in the complex plane. We determine properties of the widely linear complex OU process, including the conditions for stationarity, and the geometrical structure of the elliptical oscillations. We derive the analytical form of the power spectral density function, which then provides an efficient procedure for parameter inference using the Whittle likelihood. We apply the process to measure periodic and elliptical properties of Earth’s polar motion, including that of the Chandler wobble, for which the standard complex OU process was originally proposed.

©2020 IEEE. Personal use of this material is permitted. Permission from IEEE must be obtained for all other uses, in any current or future media, including reprinting/republishing this material for advertising or promotional purposes, creating new collective works, for resale or redistribution to servers or lists, or reuse of any copyrighted component of this work in other works.

## I. INTRODUCTION

THE signal processing community has recently given focused attention to the widely linear modelling of signals; see, e.g. [1]–[6]. The motivation for using widely linear representations is their natural ability to capture *impropriety* or *noncircularity* in complex-valued signals [7], which are ubiquitously observed across physical applications including oceanography [8] and seismology [3]. Thus far, the literature on widely linear modelling has primarily focused on discrete-time modelling. In many physical applications however, it is preferable to model the evolution of a signal in continuous time, because this allows explicit connections to be made with underlying dynamical equations, such that parameters are more physically interpretable. In this paper we propose a novel widely linear continuous-time process based on the Ornstein-Uhlenbeck (OU) process, which generates elliptical oscillations in the complex-valued signal.

A. M. Sykulski is with the Department of Mathematics and Statistics and the Data Science Institute, Lancaster University, Bailrigg, Lancaster, LA1 4YW, UK (email: a.sykulski@lancaster.ac.uk)

S. C. Olhede is with the École Polytechnique Fédérale de Lausanne, Route Cantonale, 1015 Lausanne, Switzerland (email: sofia.olhede@epfl.ch)

H. M. Sykulska-Lawrence is with the University of Southampton, Southampton, SO17 1BJ, UK (email: H.M.Sykulska-Lawrence@soton.ac.uk)

Continuous-time widely linear signal processing has previously been considered in the context of simulation [9] and estimation [10]. This paper proposes, to our knowledge, the first continuous-time widely linear model built directly from a stochastic differential equation definition (1). As we shall see, our widely linear complex OU process makes explicit connections with physical and geometric properties of the complex-valued signal.

The real-valued OU process, introduced in 1930 by Uhlenbeck and Ornstein [11], is one of the canonical continuous-time stochastic processes used across physical sciences and mathematical finance. The process can be thought of as a *damped* random walk, where the effect of the damping parameter ensures that the process is stationary over time, while maintaining the *Markov* property of random walks such that future values of the process are conditionally independent of past values given the present value.

In 1962, Arató et al. [12] introduced the *complex* Ornstein-Uhlenbeck process. Here the signal is modelled to be complex valued, and the addition of a spin parameter makes the process map out stochastic circular oscillations when viewed in the complex plane. Arató et al. [12] then fitted the process to the Chandler wobble of Earth’s polar motion—a small oscillatory deviation in the Earth’s axis of rotation relative to the solid earth—and a frequency and damping parameter of this oscillation was estimated. The complex OU process has also been used to study rotating phenomena in ocean surface flow [13], [14].

In many applications, oscillations in complex-valued signals are often observed to be elliptical, for example in seismology [3], oceanography [15], and indeed the Chandler wobble of Mars [16]. Motivated by this, in this paper we generalise Arató’s complex OU process to a widely linear form, which generates elliptical stochastic oscillations with complex dynamics, as we shall demonstrate in Section II. We will find conditions for stationarity and derive the analytical form of the power spectral density of the widely linear process. In Section III we then use this power spectral density to provide a parameter estimation procedure using a semi-parametric form of Whittle’s likelihood [14].

Inspired by Arató et al. [12], in Section IV we revisit the problem of modelling Earth’s polar motion and the Chandler wobble, while making use of over 50 years’ worth of new observational data. We first fit the standard circular complex OU process of Arató to the Chandler wobble to provide updated estimates of the frequency and damping parameters. Then we use our widely linear model to estimate and examine the presence of elliptical oscillations, both in the Chandler

wobble and the annual deviations present in the complex-valued signal. We finish with a short discussion and concluding remarks in Section V.

## II. THE WIDELY LINEAR COMPLEX OU PROCESS

Consider a complex-valued continuous-time signal given by  $z(t) = x(t) + iy(t)$ , where  $i \equiv \sqrt{-1}$  and the evolution of  $z(t)$  is defined by the following stochastic differential equation

$$dz(t) = (-\alpha_1 + i\beta_1)z(t)dt + (-\alpha_2 + i\beta_2)z^*(t)dt + dW(t), \quad (1)$$

where  $z^*(t)$  is the complex conjugate of  $z(t)$ . The parameters  $\{\alpha_1, \beta_1, \alpha_2, \beta_2\}$  are real-valued, and we shall place constraints on these parameters which ensure  $z(t)$  is stationary in Section II-B.  $W(t)$  is a Wiener process, whose increments follow a complex normal distribution with mean zero such that  $B = \{W(t + \delta) - W(t)\}/\sqrt{\delta} \sim \mathcal{CN}(0, \sigma^2, r)$ , where  $\sigma^2 = E(BB^*)$  defines the variance of the complex normal, and  $r = E(B^2)$  defines the *pseudo*-variance and is a complex-valued quantity in general (see [7]). If we set  $\alpha_2 = \beta_2 = r = 0$  then we recover the regular complex OU process of [12]. Equation (1) specifies genuine complex dynamics in a signal using a stochastic differential equation approach. We shall call (1) the widely linear complex OU process.

### A. Euler-Maruyama Generation

The widely linear complex OU process (1) is a continuous-time process, but can be accurately simulated over short discrete-time intervals by using the Euler-Maruyama scheme. Specifically, by setting  $\delta$  to be some small number, then a sequence can be generated using the iterative relationship

$$z(t + \delta) = (1 - \alpha_1\delta + i\beta_1\delta)z(t) + (-\alpha_2\delta + i\beta_2\delta)z^*(t) + \sqrt{\delta}W,$$

where  $W$  represents independent draws from  $\mathcal{CN}(0, \sigma^2, r)$ . To simulate a stationary series then the initial value should be randomly generated from a complex normal with mean zero and long-term variance and pseudo-variance, or a period of burn-in should be used. The increment  $\delta$  should be set as close as possible to zero to make the approximation more accurate.

In Fig. 1 we show two realisations of the process under two different sets of parameters, along with their empirical power spectral densities. We overlay their theoretical power spectral density whose functional form will be derived in Section II-C. As can be seen from the figure, the process generates elliptical oscillations with differing eccentricities, orientations and rates of damping. These oscillations create two peaks in the power spectral density, located at the same corresponding negative and positive frequency. In the next section we shall determine how the parameters exactly determine the properties of the elliptical oscillations, by relating the process to a bivariate vector OU process.

### B. Relationship to Bivariate OU Processes

We start by defining the *circular* real-valued bivariate OU process (see also [13]) given by

$$\begin{bmatrix} d\tilde{x}(t) \\ d\tilde{y}(t) \end{bmatrix} = \begin{bmatrix} -\alpha & -\beta \\ \beta & -\alpha \end{bmatrix} \begin{bmatrix} \tilde{x}(t) \\ \tilde{y}(t) \end{bmatrix} dt + \frac{A}{\sqrt{2}} \begin{bmatrix} dW_1(t) \\ dW_2(t) \end{bmatrix}, \quad (2)$$

where  $\alpha > 0$  ensures stationarity,  $\beta \in \mathbb{R}$  sets the frequency of the circular oscillation, and  $dW_1(t)$  and  $dW_2(t)$  are independent real-valued Wiener process increments such that  $\{W_1(t + \delta) - W_1(t)\}/\sqrt{\delta} \sim \mathcal{N}(0, 1)$  and  $\{W_2(t + \delta) - W_2(t)\}/\sqrt{\delta} \sim \mathcal{N}(0, 1)$ . We refer the reader to [17] for a more general overview of multivariate OU processes. Setting  $\tilde{z}(t) = \tilde{x}(t) + i\tilde{y}(t)$  recovers the complex OU process of [12]. In other words, (1) and (2) are equivalent when  $\alpha_1 = \alpha$ ,  $\beta_1 = \beta$ ,  $\sigma^2 = A^2$ , and  $\alpha_2 = \beta_2 = r = 0$ .

To create elliptical oscillations, we now transform (2) to create an *elliptical* bivariate OU process given by

$$\begin{bmatrix} x(t) \\ y(t) \end{bmatrix} = QP \begin{bmatrix} \tilde{x}(t) \\ \tilde{y}(t) \end{bmatrix}, \quad (3)$$

where

$$Q = \begin{bmatrix} \cos \psi & -\sin \psi \\ \sin \psi & \cos \psi \end{bmatrix}, \quad P = \begin{bmatrix} \frac{1}{\rho} & 0 \\ 0 & \rho \end{bmatrix}.$$

The parameter  $\rho$  is a stretching parameter, and  $\psi$  is a rotation parameter, which respectively set the eccentricity and orientation of the elliptical oscillations. For uniqueness we restrict  $0 < \rho \leq 1$  and  $-\pi/2 \leq \psi \leq \pi/2$ . Note that  $P$  must be applied first in (3) for  $Q$  to have an effect.

We now set  $z(t) = x(t) + iy(t)$  and show this can be written in the form of the widely linear complex OU of (1). By combining (2) and (3) we have that

$$\begin{bmatrix} dx(t) \\ dy(t) \end{bmatrix} = QP \left\{ \Omega P^{-1} Q^T \begin{bmatrix} x(t) \\ y(t) \end{bmatrix} dt + \frac{A}{\sqrt{2}} \begin{bmatrix} dW_1(t) \\ dW_2(t) \end{bmatrix} \right\}, \quad (4)$$

where

$$\Omega = \begin{bmatrix} -\alpha & -\beta \\ \beta & -\alpha \end{bmatrix},$$

and where we use that  $Q^{-1} = Q^T$ . As  $z(t) = x(t) + iy(t)$  we can define the relationship

$$\begin{bmatrix} x(t) \\ y(t) \end{bmatrix} = \frac{1}{2} T \begin{bmatrix} z(t) \\ z^*(t) \end{bmatrix}, \quad T = \begin{bmatrix} 1 & 1 \\ -i & i \end{bmatrix}. \quad (5)$$

By combining (4) and (5) we obtain

$$\begin{bmatrix} dz(t) \\ dz^*(t) \end{bmatrix} = \frac{1}{2} T^H L T \begin{bmatrix} z(t) \\ z^*(t) \end{bmatrix} dt + T^H Q P \frac{A}{\sqrt{2}} \begin{bmatrix} dW_1(t) \\ dW_2(t) \end{bmatrix}, \quad (6)$$

where  $L = QP\Omega P^{-1}Q^T$ . The widely linear complex OU SDE is then obtained from expanding (6) and taking the top row, such that we obtain

$$\begin{aligned} dz(t) = & \left( -\alpha + i\frac{\beta}{2} \left\{ \frac{1}{\rho^2} + \rho^2 \right\} \right) z(t)dt \\ & + \frac{\beta}{2} \left\{ \frac{1}{\rho^2} - \rho^2 \right\} (\sin 2\psi - i \cos 2\psi) z^*(t)dt + dW(t), \end{aligned} \quad (7)$$

where the increment process  $dW(t)$  is defined by

$$\sigma^2 = \frac{A^2}{2} \left( \frac{1}{\rho^2} + \rho^2 \right), \quad r = \frac{A^2}{2} \left( \frac{1}{\rho^2} - \rho^2 \right) e^{i2\psi}.$$

By equating the parameters in (1) and (7) we can obtain an exact one-to-one mapping between the parameter set  $\{\alpha_1, \beta_1, \alpha_2, \beta_2, \sigma^2\}$  of the widely linear complex OU of

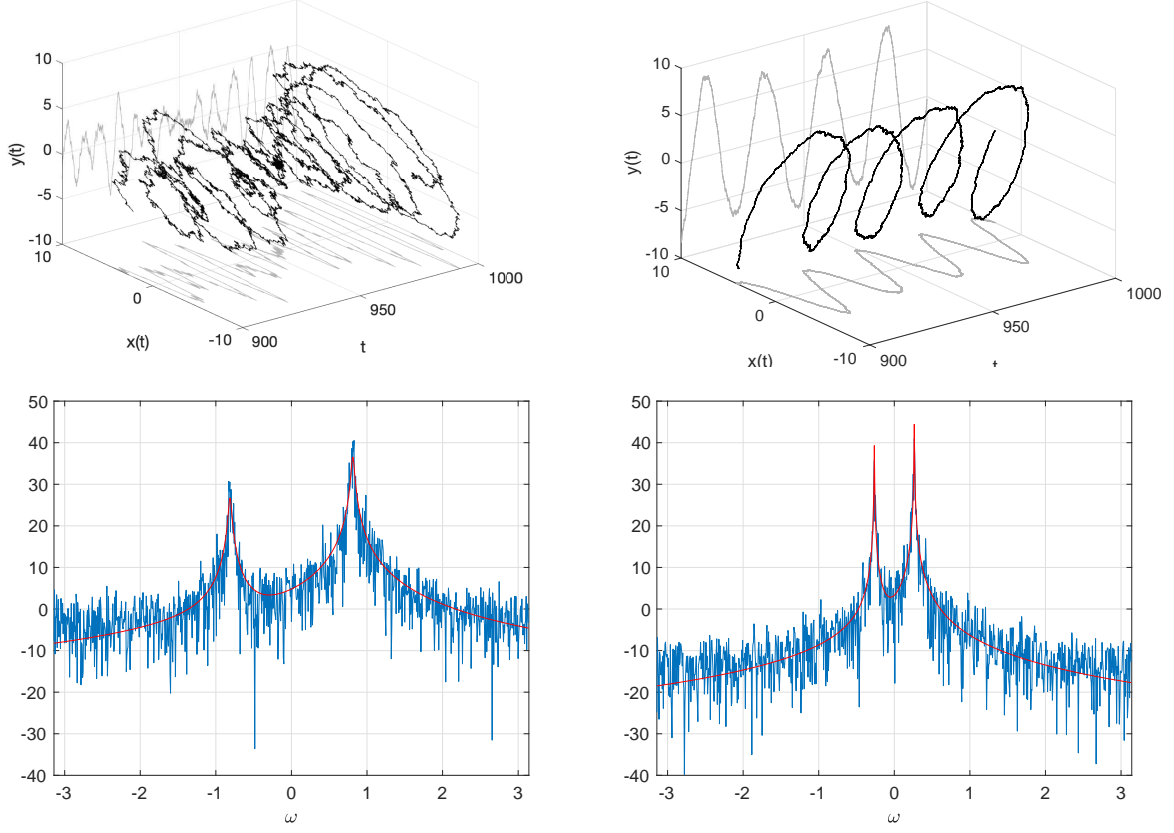


Fig. 1. The top row displays two realisations of the widely linear complex OU process  $z(t) = x(t) + iy(t)$  of (1) with parameters  $\{\alpha_1 = 0.2, \beta_1 = 1, \alpha_2 = -0.5, \beta_2 = -0.3, \sigma^2 = 2, r = 0.6 + i\}$  (left) and  $\{\alpha_1 = 0.02, \beta_1 = 0.5, \alpha_2 = 0.3, \beta_2 = 0.3, \sigma^2 = 0.15, r = -0.09 - 0.09i\}$  (right) generated using the Euler-Maruyama scheme. We plot  $z(t)$  in black, and the  $x(t)$  and  $y(t)$  components in grayscale in the 3D plot. We set  $\delta = 1/1000$  and simulate from  $t = 0$  to  $t = 1000$  and plot both signals from  $t = 900$  to  $t = 1000$  only. In the bottom row we display the empirical periodograms of the full length signals (on a decibel scale), and overlay the theoretical power spectral from (9) in red. The slight discrepancy at the highest frequencies is due to aliasing effects on the periodogram.

(1), and the parameter set  $\{\alpha, \beta, \rho, \psi, A^2\}$  of the elliptical bivariate OU of (3). The mapping in each direction is given in Table I. The parameter  $r$ , which sets the pseudo-variance of the complex-valued increment process  $dW(t)$ , is redundant and should be set as

$$r = -\frac{\sigma^2}{\beta_1}(\beta_2 + i\alpha_2),$$

such that the widely linear complex OU is reduced to five free parameters from mapping to an elliptical bivariate OU process. Setting  $\rho = 1$  in (7) (and Table I) recovers the regular three-parameter complex OU process of [12] and (2).

In the widely linear setting, we observe from Table I the simple relationship that  $\alpha_1 = \alpha$ , meaning these parameters set the respective damping rates of the oscillations in each process, and we thus require  $\alpha_1 > 0$  for the widely linear complex OU to be stationary. The parameters  $\{\beta_1, \alpha_2, \beta_1\}$  jointly determine  $\{\beta, \rho, \psi\}$  (the oscillation frequency, eccentricity and orientation) and we require  $|\beta_1| > \sqrt{\alpha_2^2 + \beta_2^2}$  to create a valid mapping between the two processes. The eccentricity of the oscillations is given by

$$\varepsilon = \sqrt{1 - \rho^4} = \sqrt{\frac{2\sqrt{\alpha_2^2 + \beta_2^2}}{|\beta_1| + \sqrt{\alpha_2^2 + \beta_2^2}}},$$

TABLE I  
THIS TABLE PROVIDES A MAPPING BETWEEN THE PARAMETERS OF THE WIDELY LINEAR COMPLEX OU (1) AND THE ELLIPTICAL BIVARIATE OU (3). THE FUNCTION `atan2` IS THE FOUR QUADRANT INVERSE TANGENT AND `sgn` IS THE SIGNUM FUNCTION.

Bivariate to Complex	Complex to Bivariate
$\alpha_1 = \alpha$	$\alpha = \alpha_1$
$\beta_1 = \frac{\beta}{2} \left( \rho^2 + \frac{1}{\rho^2} \right)$	$\beta = \text{sgn}(\beta_1) \sqrt{\beta_1^2 - \alpha_2^2 - \beta_2^2}$
$\alpha_2 = \frac{\beta}{2} \left( \rho^2 - \frac{1}{\rho^2} \right) \sin 2\psi$	$\rho = \left( \frac{ \beta_1  - \sqrt{\alpha_2^2 + \beta_2^2}}{ \beta_1  + \sqrt{\alpha_2^2 + \beta_2^2}} \right)^{1/4}$
$\beta_2 = \frac{\beta}{2} \left( \rho^2 - \frac{1}{\rho^2} \right) \cos 2\psi$	$\psi = \frac{\text{sgn}(-\beta_1)}{2} \text{atan2}(\alpha_2, \text{sgn}(-\beta_1)\beta_2)$
$\sigma^2 = \frac{A^2}{2} \left( \rho^2 + \frac{1}{\rho^2} \right)$	$A^2 = \sigma^2 \frac{\sqrt{\beta_1^2 - \alpha_2^2 - \beta_2^2}}{ \beta_1 }$

such that larger values of  $\alpha_2$  and  $\beta_2$  create more eccentric oscillations. In the next section we derive the power spectral density of the widely linear complex OU which will provide further intuition on the effect of the different parameters.

A similar mapping analysis was performed with discrete-time models in [3] by equating a widely linear autoregressive

AR(1) process to a corresponding bivariate process. The mappings between the parameters are significantly different here as compared with those found in [3] for discrete time. There are two reasons why these mappings are so different. First, although an AR(1) process can generally be interpreted as a discrete-time analogue of an OU process, there is no simple transformation between their sets of parameters in the widely linear case, as we show in Appendix A. This is consistent with [18] which discusses the nontrivial relationship between sampled CARMA (continuous ARMA) models and regular discrete-time ARMA models. Secondly, the widely linear complex OU process of (1) has coefficients given in Cartesian form, whereas the coefficients of the widely linear AR(1) are given in polar form (see (15) in Appendix A). These parameterisations in each case make sense as the mappings between the OU and AR processes are then straightforward in the regular (non widely linear) case, see (16)–(18) in Appendix A. However, these choices of parameterisations cause further departures in the parameter mappings in the widely linear case. As a result, the conditions for stationarity, and the geometrical properties of elliptical oscillations, are entirely different in the continuous-time complex OU proposed in this paper, and the discrete-time AR(1) proposed in [3].

### C. The Power Spectral Density

For stationary complex-valued processes the power spectral density can in general be defined from the autocovariance sequence of the process, such that

$$S_z(\omega) = \int s_z(\tau) e^{-i\omega\tau} d\tau, \quad s_z(\tau) = \mathbb{E}\{z(t)z^*(t+\tau)\}.$$

The power spectral density of the regular complex OU process of [12] is given by [14]

$$S_z(\omega) = \frac{\sigma^2}{\alpha_1^2 + (\omega - \beta_2)^2} = \frac{A^2}{\alpha^2 + (\omega - \beta)^2}, \quad (8)$$

which we have provided both in terms of the parameterization of (1) (with  $\alpha_2 = \beta_2 = r = 0$ ), and of the circular bivariate process of (2).

The power spectral density of the widely linear complex OU process is given by

$$S_z(\omega) = A^2 \left\{ \frac{\left(\frac{1}{\rho} + \rho\right)^2}{\alpha^2 + (\omega - \beta)^2} + \frac{\left(\frac{1}{\rho} - \rho\right)^2}{\alpha^2 + (\omega + \beta)^2} \right\}, \quad (9)$$

which is given in terms of the parametrisation of the elliptical bivariate process of (3). Then to find the power spectral density in terms of (1) one simply substitutes using the transformations in the right column of Table I. The derivation of (9) is provided in Appendix B.

Intuition is gained by examining (9). While (8) has just one peak in the spectral density located at  $\omega = \beta$ , (9) has two peaks located at  $\omega = \pm\beta$ . The rate of damping of both peaks is determined by  $\alpha$ , and the ratio of magnitudes of the two peaks is determined by  $\rho$ . Note that the orientation parameter  $\psi$  does not feature in the power spectral density. When (9) is represented using the parameters of (1) then

we see that  $\alpha_1$  defines the damping of the two peaks, and  $\{\beta_1, \alpha_2, \beta_2\}$  together determine the peak locations and their relative magnitudes. We have overlaid the power spectral density of (9) over the periodogram of the simulated series in Fig. 1.

To fully specify the properties of the widely linear complex OU process, we also need to derive the *complementary* spectrum defined by

$$R_z(\omega) = \int r_z(\tau) e^{-i\omega\tau} d\tau, \quad r_z(\tau) = \mathbb{E}\{z(t)z(t+\tau)\}.$$

The regular complex OU process of [12] is a *proper* process and therefore  $R_z(\omega) = r_z(\tau) = 0$ . The widely linear complex OU is an *improper* process and the complementary spectrum is given by

$$R_z(\omega) = \frac{A^2}{4} \left( \frac{1}{\rho^2} - \rho^2 \right) \times \left\{ \frac{1}{\alpha^2 + (\omega - \beta)^2} + \frac{1}{\alpha^2 + (\omega + \beta)^2} \right\} e^{i2\psi}, \quad (10)$$

which is dependent on  $\psi$ , as well as all the other parameters. Setting  $\rho = 1$  recovers  $R_z(\omega) = 0$  as expected. The derivation of (10) can also be found in Appendix B. We note that full specification of the power spectral density and complementary spectrum allows for an exact method of simulation based on circular embedding and Fourier transforms, as an alternative to Euler-Maruyama, see [19] for details.

## III. PARAMETER ESTIMATION

In this section we show how to estimate parameters of (1) from a length- $n$  observed complex-valued signal  $\mathbf{Z} = [Z_1, \dots, Z_n]$  where the signal is regularly sampled at intervals denoted by  $\Delta$ .

### A. The Whittle likelihood

The Whittle likelihood is an approximation to the log-likelihood, and was found for complex-valued signals in [8] and is given by

$$\ell_W(\theta) = - \sum_{\omega \in \Omega} \{ \log |S_C(\omega; \theta)| + J_C^H(\omega) S_C^{-1}(\omega; \theta) J_C(\omega) \}, \quad (11)$$

where

$$J_C(\omega) = \begin{bmatrix} J_Z(\omega) \\ J_{Z^*}(\omega) \end{bmatrix} = \frac{\sqrt{\Delta}}{N} \sum_{t=1}^n \begin{bmatrix} Z_t \\ Z_t^* \end{bmatrix} e^{-i\omega t \Delta},$$

is the Discrete Fourier Transform of  $[Z_t \ Z_t^*]^T$ , and

$$S_C(\omega; \theta) = \begin{bmatrix} S_z(\omega; \theta) & R_z(\omega; \theta) \\ R_z^*(\omega; \theta) & S_z(-\omega; \theta) \end{bmatrix},$$

where  $|S_C(\omega; \theta)|$  denotes the determinant of matrix  $S_C(\omega; \theta)$ . The set of Fourier frequencies  $\Omega$  in (11) is given by

$$\Omega = \frac{2\pi}{n\Delta} (-\lceil n/2 \rceil + 1, \dots, -1, 0, 1, \dots, \lfloor n/2 \rfloor). \quad (12)$$

The widely linear complex OU parameters can therefore be estimated by substituting (9) and (10) in (11) and then maximising  $\ell_W(\theta)$  over the parameter vector  $\theta = \{\alpha, \beta, \rho, \psi, A^2\}$  to find the Whittle likelihood estimate. This estimate can then be transformed into the parameters of (1) using Table I.



### B. Semi-parametric Whittle likelihood

An alternative method, more suited to certain applications, is to only fit the power spectral density, and not the complementary spectrum. This then becomes a *semi-parametric* Whittle likelihood estimate and is given by the simple form

$$\ell_S(\theta) = - \sum_{\omega \in \Omega} \left\{ \log S_z(\omega; \theta) + \frac{I_Z(\omega)}{S_z(\omega; \theta)} \right\}, \quad (13)$$

where  $I_Z(\omega) = |J_Z(\omega)|^2$  is the periodogram of the observed signal. The likelihood estimate can be made even more semi-parametric by only including a subset of frequencies from (12) in the Whittle fit of (13) (see also [20]). This can be useful when the periodogram is contaminated by high frequency noise (and high frequencies should hence be excluded from the fit), or the chosen model is known to only be correct in a narrow range of frequencies, perhaps because an aggregation of effects has been observed. Indeed we shall employ semi-parametric Whittle fits in Section IV to separate the annual and Chandler wobble oscillations of Earth's polar motion.

To fit the widely linear complex OU, we simply substitute (9) into (13) and maximise  $\ell_S(\theta)$  to find the semi-parametric Whittle estimates. We note that this can only be done over the parameter vector  $\theta = \{\alpha, \beta, \rho, A^2\}$  as  $\psi$  is not present in the power spectral density of (9). We therefore propose the following nonparametric estimate

$$\hat{\psi} = \frac{1}{2} \left[ \arg\{J(\hat{\beta})\} + \arg\{J(-\hat{\beta})\} \right], \quad (14)$$

where  $\hat{\beta}$  is the semi-parametric Whittle estimate of  $\beta$  from maximising (13). Again, the parameter estimates corresponding to (1) are found using the right column of Table I.

Other modifications to Whittle likelihood including tapering and differencing the signal, or debiasing the estimates to account for aliasing and spectral blurring (see [21] for a review). We did not find such modifications to be needed for the widely linear complex OU process. This is because the process has a relatively small dynamic range, owing to the  $\omega^{-2}$  decay in (9), such that there is only a small amount of spectral blurring present in the periodogram.

## IV. EARTH'S POLAR MOTION

In Fig. 2 we plot Earth's polar motion from 1845 to present day, measured in milliarcseconds (mas). The data is publicly available from the International Earth Rotation and Reference Systems Service Earth Orientation products<sup>1</sup>. We can observe a slow drift in the signal, especially in the  $y$  axis, coupled with clear oscillatory deviations.

In Fig. 3 we plot the periodogram of the complex-valued signal  $z(t) = x(t) + iy(t)$ . For complex-valued signals, the periodogram is in general asymmetric over positive and negative frequencies, as directions of spin are separated in complex-valued signal modelling. Negative frequencies correspond to clockwise oscillations and positive frequencies correspond to anti-clockwise oscillations. In Fig. 3 we detect three clear peaks in the signal. The largest at frequency zero is due to

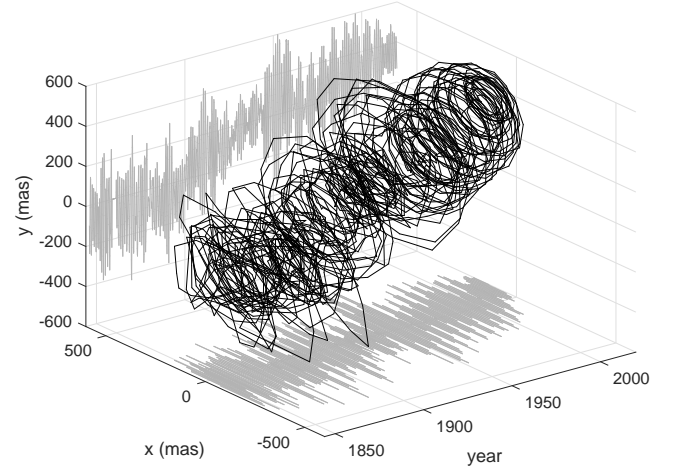


Fig. 2. Earth's polar motion from 1845 to present day, measured in regular intervals of 0.1 years.

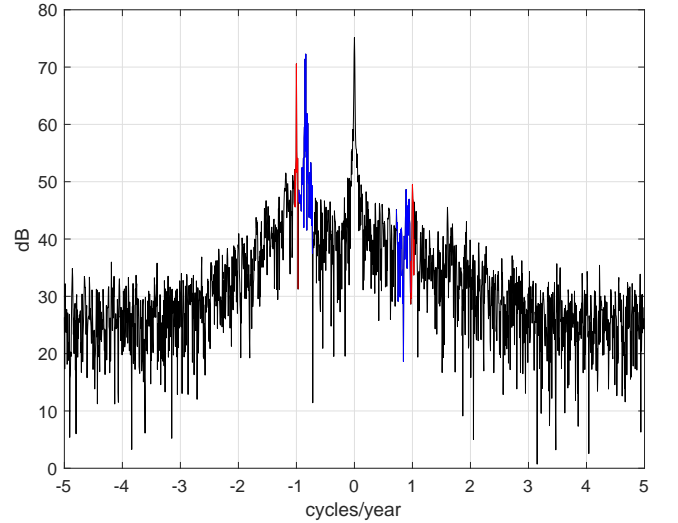


Fig. 3. The periodogram of Earth's polar motion of Fig. 2 when represented as a complex-valued signal. The red band of frequencies corresponds to the annual oscillation, and the blue band to the Chandler wobble.

the drift. The smallest, at (negative) one cycle per year, is the annual oscillation. The third, at approximately -0.84 cycles per year is the Chandler wobble, discovered by astronomer Seth Carlo Chandler in 1891.

We will study the properties of both oscillations using the widely linear complex OU (1). To do this we cannot only look at the precise values and locations of the peaks in the spectral density, but we also need to consider frequencies in the *vicinity* of the peaks, such that we can estimate the damping parameter  $\alpha_1$  of the oscillations. We have marked in blue and red (respectively) the frequencies we will use to model the Chandler and Earth wobble oscillations respectively. Specifically, the Chandler Wobble is considered in the range -0.73 to -0.96 cycles per year, and the annual oscillation in the range -0.965 to -1.035 cycles per year. We have also marked the corresponding positive frequencies, which will contained some elevated power if this component of the signal has elliptical structure.

<sup>1</sup> [www.iers.org/IERS/EN/DataProducts/EarthOrientationData/eop.html](http://www.iers.org/IERS/EN/DataProducts/EarthOrientationData/eop.html)

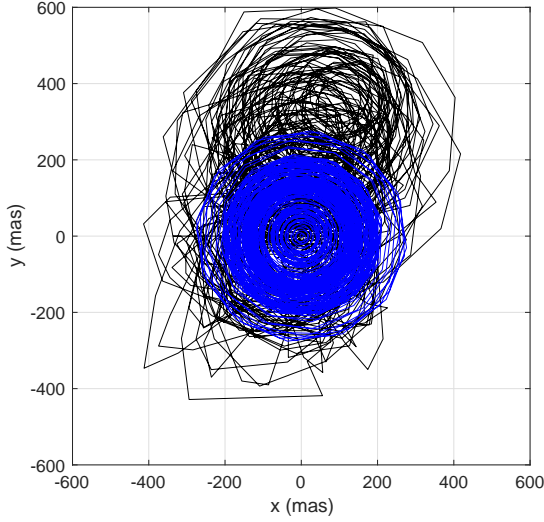


Fig. 4. The Chandler wobble in the complex plane (in blue), which has been bandpass filtered from Fig. 2 using the frequencies highlighted in Fig. 3 (negative frequencies only). The full signal of Fig. 2 is plotted in black.

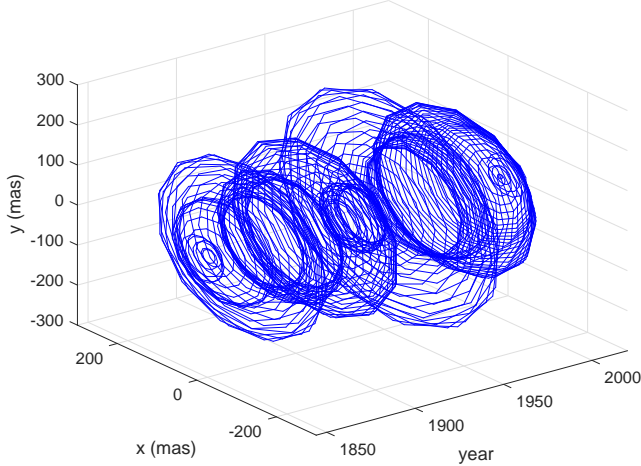


Fig. 5. The Chandler wobble over time, which has been bandpass filtered from Fig. 2 using the frequencies highlighted in Fig. 3 (negative frequencies only).

We now bandpass filter the negative blue frequencies in Fig. 3 corresponding to the Chandler wobble, and plot these in blue on the complex plane in Fig. 4. We overlay the full polar motion signal in black. As we have only filtered the negative frequency, then the oscillations appear entirely circular. We display the same filtered signal on a 3-D plot in Fig. 5, where the varying amplitude of the signal can be clearly seen. This suggests the presence of damping in the oscillation, and motivated the construction of the regular complex OU by Arató in [12]. Next in Fig. 6 we display the bandpassed polar motion signal over both negative and positive frequencies in blue from Fig. 3. No clear ellipticity can be observed by eye, but we will study this in more detail using the widely linear complex OU shortly.

First we show the bandpass filtered annual oscillations corresponding to the red frequencies in Fig. 2, over both negative and positive frequencies. These are displayed in

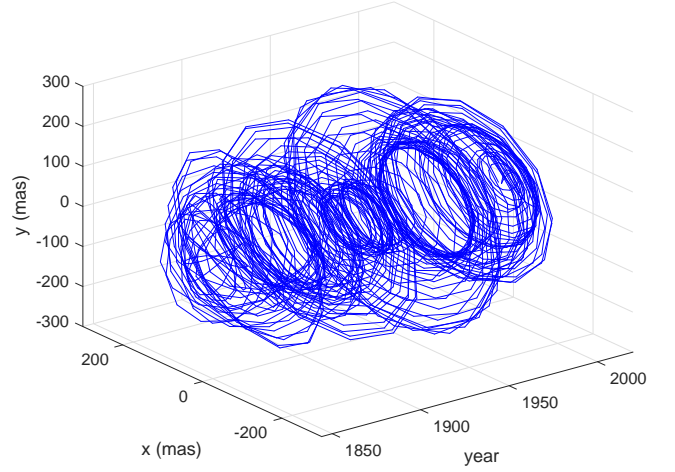


Fig. 6. The Chandler wobble over time, which has been bandpass filtered from Fig. 2 using the frequencies highlighted in Fig. 3 (using both positive and negative frequencies).

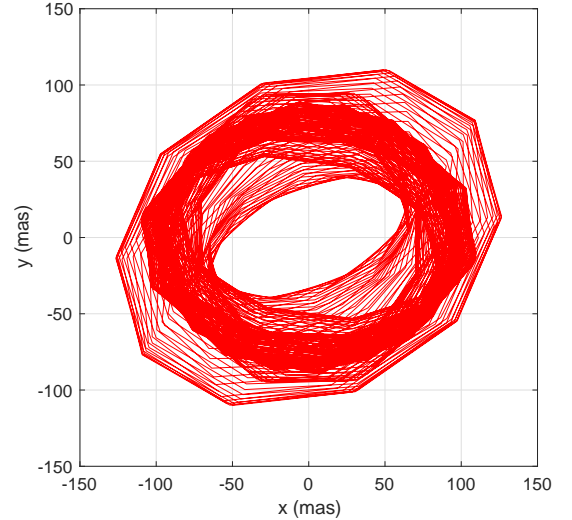


Fig. 7. The annual oscillation in the complex plane, which has been bandpass filtered from Fig. 2 using the frequencies highlighted in Fig. 3 (using both positive and negative frequencies).

Figs. 7 and 8 respectively in the 2D and 3D perspectives. The ellipticity of the signal is much clearer this time, and again we will investigate this in more detail using the widely linear complex OU process.

We now fit complex OU processes to the data. First, we consider the Chandler Wobble over negative frequencies only and fit the regular complex OU of Arató [12], which corresponds to the widely linear complex OU (1) when  $\alpha_2 = \beta_2 = r = 0$ . We fit the parameters using the semi-parametric Whittle procedure described in Section III-B. The fit of the power spectral density of the regular complex OU in (8) to the periodogram is displayed in Fig. 9. Although the periodogram is variable, it lies within the 95% confidence intervals of the modelled power spectral density almost everywhere. Confidence intervals are estimated using the asymptotic chi-squared distribution of the periodogram. The estimated parameters (to 3 significant figures) are  $\alpha_1 = 0.0425$  (in units of  $\text{years}^{-1}$ ),  $\beta_1 = -0.842$

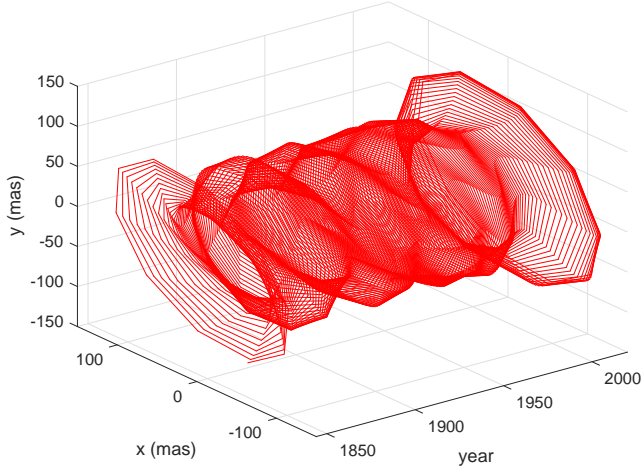


Fig. 8. The annual oscillation over time, which has been bandpass filtered from Fig. 2 using the frequencies highlighted in Fig. 3 (using both positive and negative frequencies).

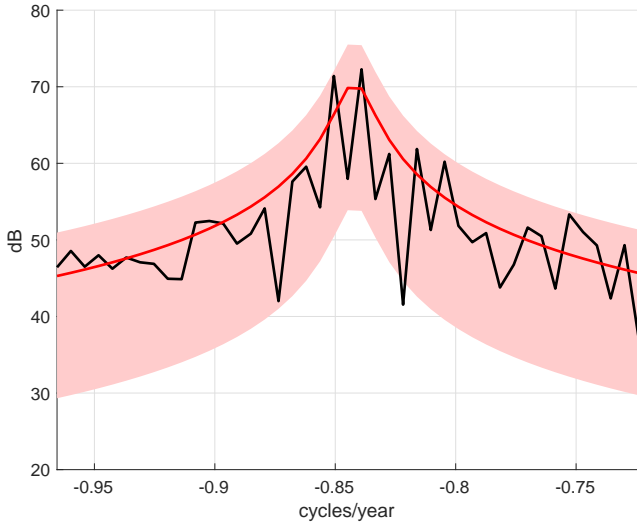


Fig. 9. The fit of the power spectral density of the circular complex OU process (red) to the periodogram of Earth's polar motion (black). The fit is performed semi-parametrically using the Whittle likelihood in the frequency interval of  $-0.96$  to  $-0.73$  cycles per year which captures the Chandler wobble. 95% confidence intervals of the power spectral density are in red shading.

(cycles per year) and  $\sigma^2 = 204$ .

Arató [12], in his 1962 analysis, found  $\alpha_1 = 0.09$  and  $\beta_1 = -0.839$ , but the 95% confidence range for  $\alpha_1$  was found to be  $[0.01, 0.1]$  which is consistent with our estimate. So our estimates, which utilise over 50 years of new data, are in broad agreement with Arató but we find a slightly lower damping parameter. We note however that information about the damping parameter lies over very few frequencies, and is therefore a challenging parameter to estimate. This observation was also made by [12] (hence the wide confidence intervals). In other literature, Brillinger [22] also uses a regular complex OU process like Arató, but makes some seasonal corrections, and finds  $\alpha_1 = 0.06$  cycles per year with a 95% confidence range of  $[0.006, 0.114]$ . More broadly, there still remains an active research debate on the rate of damping of the Chandler wobble [23], where a variety of geophysical models have been

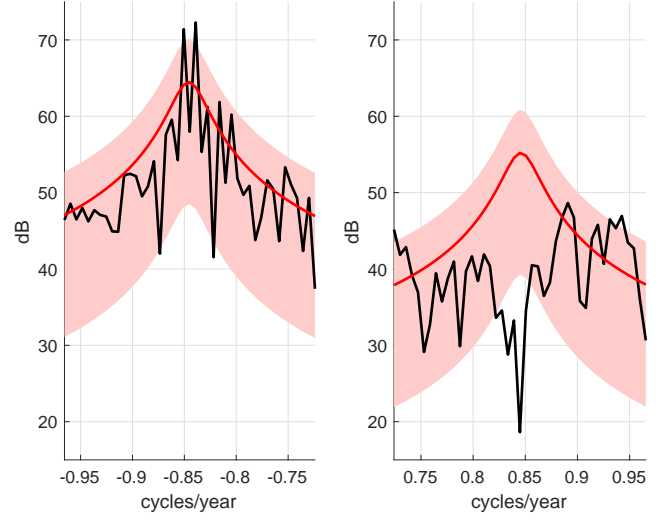


Fig. 10. The fit of the power spectral density of the widely linear complex OU process (red) to the periodogram of Earth's polar motion (black). The fit is performed semi-parametrically using the Whittle likelihood in the frequency intervals of  $-0.96$  to  $-0.73$  and  $0.73$  to  $0.96$  cycles per year, which captures the (elliptical) Chandler wobble. 95% confidence intervals of the power spectral density are in red shading.

employed to measure this, but a more detailed comparison with this literature is far beyond the scope of this paper.

Now we fit the widely linear complex OU to the Chandler wobble over negative and positive frequencies. We again use the semi-parametric Whittle procedure. The fits are displayed in Fig. 10. Clearly the fit to positive frequencies is poor, with no clear peak in the periodogram, and several values lying outside of the 95% confidence range at several frequencies near the peak. This is consistent with the literature where the Chandler wobble motion has been described as “*quasi-circular*” with a low eccentricity in the range  $[0.1, 0.23]$  in [24]. The periodogram of the signal is too variable and is contaminated by other artefacts at the positive frequencies, so our model is unable to detect this low eccentricity in the Chandler wobble oscillation for this reason.

Instead we now fit the widely linear complex OU to the annual oscillation over negative and positive frequencies. The fits are displayed in Fig. 11, and this time the model is a much better fit, even though the range of frequencies over which the fit can be performed is relatively narrow. The periodogram comfortably lies within the 95% confidence interval bands at all modelled frequencies. The estimated parameters (to 3 significant figures) are  $\{\alpha = 0.0193, \beta = -1.00, \rho = 0.793, \psi = 0.122, A^2 = 21.0\}$  in the bivariate representation of (3) and  $\{\alpha_1 = 0.0193, \beta_1 = -1.11, \alpha_2 = 0.116, \beta_2 = 0.476, \sigma^2 = 23.3, r = 9.82 + i2.44\}$  in the widely linear complex OU representation of (1). As discussed in Section III-B, the orientation parameter  $\psi$  cannot be estimated using the semi-parametric Whittle technique and is instead estimated using (14). The eccentricity of the annual oscillation is estimated to be  $\varepsilon = \sqrt{1 - \rho^4} = 0.777$ . This is in broad agreement but slightly different from [24] who discover a “significantly elliptic annual motion” in the range  $[0.26, 0.49]$ . For comparison, a simple non-parametric estimate from the

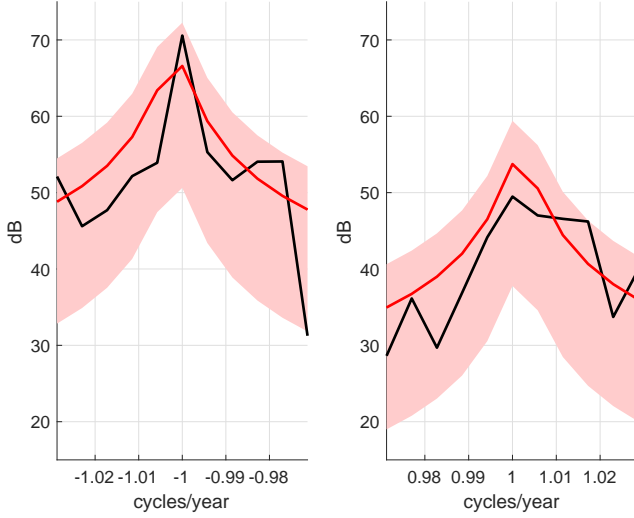


Fig. 11. The fit of the power spectral density of the widely linear complex OU process (red) to the periodogram of Earth's polar motion (black). The fit is performed semi-parametrically using the Whittle likelihood in the frequency intervals of  $-1.035$  to  $-0.965$  and  $0.965$  to  $1.035$  cycles per year, which captures the (elliptical) annual oscillation. 95% confidence intervals of the power spectral density are in red shading.

data from Fig. 2 using (see [3])

$$\hat{\varepsilon} = \frac{2\sqrt{|J_Z(\omega=1)J_Z(\omega=-1)|}}{|J_Z(\omega=1)| + |J_Z(\omega=-1)|},$$

yields  $\hat{\varepsilon} = 0.546$ . The higher values of eccentricity we estimate as compared with [24] are likely due to their approach of time-windowing into small intervals, versus our approach of considering the entire signal as a stochastic process. Again, a more detailed analysis is beyond the scope of this paper. Our example here does however serve as a proof-of-concept of the potential applications of our novel continuous-time widely linear process.

## V. DISCUSSION AND CONCLUSION

Oscillations are key features of natural and human-made phenomena. Often we observe linked oscillations that map out the same periodic phenomenon. For deterministic phenomena, such have been studied in [25]–[27], and for stochastic phenomena in [3], [14]. Continuous time signals that are improper are, as we have shown, challenging to describe but possess interpretable multidimensional dynamics [27]. The aim of this paper has been to introduce a structured form of multivariate dependence so that elliptical trajectories are mapped out, just like single oscillations can be conceptualised as mapping out circles. Complex-valued models, such as the widely linear complex OU, provide rich structural information as we can recover the geometric features of the ellipse from the observations, as is clarified by Table I.

Multivariate stochastic processes have been the focus of intensive research in the last decade [28]–[32]. There is much advantage to modelling underlying geometry in signals [33], but that viewpoint exactly corresponds as to how the underlying structure in the observations evolves over time. Oscillations are natural as a modelling starting point when

studying stationary phenomena. The multivariate generalisation of an oscillation is an observed trajectory from an ellipse [27]. This puts an emphasis on the classes of models starting from oscillations, broadening to partially observed trajectories on the ellipse.

A number of questions remain unresolved. Our generalisation of the OU model is just one example of a statistical model of temporal structure. The differential equation linkage has been discussed further for other applications including random fields by [34]. We envision that similar extensions could be done to their model classes. This would build on the non-parametric statistical work of [35]. Furthermore, we can seek similar extensions to trivariate and multivariate temporal signals, building stochastic analogues to the deterministic approaches taken in [26], [27].

Finally our understanding of the widely linear complex OU has been significantly enhanced by the analysis of polar motion and the Chandler wobble. Polar motion data has been collected from more planets than Earth and our understanding of the model would be significantly enhanced by analysing such data and testing our model on real data structures such as Mars [36], especially as richer datasets become available from future missions making such analysis more feasible. The challenges of real data examples will stress test our model, and show us what new features and geometrical structures require incorporating into the model framework.

## APPENDIX A

### RELATIONSHIP BETWEEN THE OU AND AR(1) PROCESSES

Consider the widely linear complex autoregressive process of [3] given by

$$Z(t) = \lambda e^{i\zeta} Z(t-1) + \gamma e^{i\phi} Z^*(t-1) + \epsilon_t, \quad (15)$$

with noise variance  $\sigma_{AR}^2$  and pseudo-variance  $r_{AR}$ . Let us now contrast this with the widely linear complex OU of (1). In the simple (proper) case of  $\gamma = \alpha_2 = \beta_2 = r = r_{AR} = 0$  then a regular sampled complex OU (at intervals  $\Delta$ ) is like a complex AR(1) where

$$\lambda = e^{-\alpha_1 \Delta}, \quad (16)$$

and

$$\sigma_{AR}^2 = \sigma^2 \frac{(1 - e^{-2\alpha_1 \Delta})}{2\alpha_1}, \quad (17)$$

and

$$\zeta = \beta_1, \quad (18)$$

thus providing a simple mapping between the processes. These relationships can be derived by considering an Euler-Maruyama expansion of the OU:

$$z(t + 1/x) \approx (1 - \alpha_1/x + i\beta_1/x)z(t) + \sqrt{A^2/x}B,$$

where  $x$  is large and  $B$  is a draw from a  $\mathcal{N}(0, 1)$  such that repeating  $x\Delta$  times we have

$$\begin{aligned} z(t + \Delta) &\approx (1 - \alpha_1/x + i\beta_1/x)^{x\Delta} z(t) \\ &\quad + \sqrt{A^2/x} \sum_{k=0}^{x\Delta-1} (1 - \alpha_1/x)^k B, \end{aligned}$$



and then taking  $x \rightarrow \infty$  we get the relationships above.

In the general case  $\gamma \neq \alpha_2 \neq \beta_2 \neq r \neq r_{AR} \neq 0$  then the Euler-Maruyama expansion becomes

$$z\left(t + \frac{1}{x}\right) \approx \left(1 - \frac{\alpha_1}{x} + \frac{i\beta_1}{x}\right) z(t) - \left(\frac{\alpha_2}{x} - \frac{i\beta_2}{x}\right) z^*(t) + \sqrt{\frac{1}{x}} B,$$

where  $B$  is a draw from  $\mathcal{CN}(0, \sigma^2, r)$ . Then repeating  $x\Delta$  times and taking  $x \rightarrow \infty$  we observe that

$$\lambda e^{i\zeta} = \lim_{x \rightarrow \infty} \sum_{k=0}^{x\Delta/2} \left(1 - \frac{\alpha_1}{x} + \frac{i\beta_1}{x}\right)^{x\Delta-2k} \times \left(\frac{\alpha_2}{x} - \frac{i\beta_2}{x}\right)^{2k} \binom{x\Delta}{2k},$$

and

$$\gamma e^{i\phi} = \lim_{x \rightarrow \infty} \sum_{j=1}^{x\Delta/2} \left(1 - \frac{\alpha_1}{x} + \frac{i\beta_1}{x}\right)^{x\Delta-2j+1} \times \left(\frac{\alpha_2}{x} - \frac{i\beta_2}{x}\right)^{2j-1} \binom{x\Delta}{2j-1},$$

which have no clear analytical solutions, such that we can observe the nontrivial mapping between the processes in the widely linear case.

## APPENDIX B

### POWER SPECTRAL DENSITY DERIVATION

To derive the power spectral density of the widely linear complex OU, we start from the power spectral density of the regular complex OU in (8) and convert to Cartesian forms using the relationships given in [8]

$$\begin{aligned} S_{\tilde{x}}(\omega) &= \frac{1}{4} \{S_{\tilde{z}}(\omega) + S_{\tilde{z}}(-\omega)\} + \frac{1}{2} \mathcal{R}\{R_{\tilde{z}}(\omega)\}, \\ S_{\tilde{y}}(\omega) &= \frac{1}{4} \{S_{\tilde{z}}(\omega) + S_{\tilde{z}}(-\omega)\} - \frac{1}{2} \mathcal{R}\{R_{\tilde{z}}(\omega)\}, \\ S_{\tilde{x}\tilde{y}}(\omega) &= \frac{1}{2} \mathcal{I}\{R_{\tilde{z}}(\omega)\} + \frac{i}{4} \{S_{\tilde{z}}(\omega) - S_{\tilde{z}}(-\omega)\}, \end{aligned}$$

where  $S_{\tilde{x}\tilde{y}}(\omega)$  is the cross-spectral density between  $\tilde{x}(t)$  and  $\tilde{y}(t)$ , and  $\mathcal{R}\{\cdot\}$  and  $\mathcal{I}\{\cdot\}$  denote the real and imaginary part respectively. Substituting in (8), and using that  $R_{\tilde{z}}(\omega) = 0$  as the regular complex OU is a proper process, we obtain

$$S_{\tilde{x}}(\omega) = \frac{A^2}{4} \left\{ \frac{1}{\alpha^2 + (\omega - \beta)^2} + \frac{1}{\alpha^2 + (\omega + \beta)^2} \right\}, \quad (19)$$

$$S_{\tilde{y}}(\omega) = \frac{A^2}{4} \left\{ \frac{1}{\alpha^2 + (\omega - \beta)^2} + \frac{1}{\alpha^2 + (\omega + \beta)^2} \right\}, \quad (20)$$

$$S_{\tilde{x}\tilde{y}}(\omega) = \frac{iA^2}{4} \left\{ \frac{1}{\alpha^2 + (\omega - \beta)^2} - \frac{1}{\alpha^2 + (\omega + \beta)^2} \right\}. \quad (21)$$

Note that  $S_{\tilde{x}}(\omega) = S_{\tilde{y}}(\omega)$ . Next we find the power spectral densities of the elliptical bivariate OU process. First we note by expanding (3) that

$$\begin{aligned} x(t) &= \frac{1}{\rho} \tilde{x}(t) \cos \psi - \rho \tilde{y}(t) \sin \psi, \\ y(t) &= \rho \tilde{y}(t) \cos \psi + \frac{1}{\rho} \tilde{x}(t) \sin \psi. \end{aligned}$$

This clarifies the geometric interpretation of  $P$  and  $Q$  in (3).

It then follows that

$$S_x(\omega) = \frac{\cos^2 \psi}{\rho^2} S_{\tilde{x}}(\omega) + \rho^2 \sin^2 \psi S_{\tilde{y}}(\omega) - \cos \psi \sin \psi S_{\tilde{x}\tilde{y}}(\omega) - \cos \psi \sin \psi S_{\tilde{x}\tilde{y}}^*(\omega), \quad (22)$$

$$S_y(\omega) = \frac{\sin^2 \psi}{\rho^2} S_{\tilde{y}}(\omega) + \rho^2 \cos^2 \psi S_{\tilde{x}}(\omega) + \cos \psi \sin \psi S_{\tilde{x}\tilde{y}}(\omega) + \cos \psi \sin \psi S_{\tilde{x}\tilde{y}}^*(\omega), \quad (23)$$

$$S_{xy}(\omega) = \frac{\cos \psi \sin \psi}{\rho^2} S_{\tilde{x}}(\omega) - \rho^2 \cos \psi \sin \psi S_{\tilde{y}}(\omega) + \cos^2 \psi S_{\tilde{x}\tilde{y}}(\omega) - \sin^2 \psi S_{\tilde{x}\tilde{y}}^*(\omega), \quad (24)$$

where we have used that  $S_{\tilde{y}\tilde{x}}(\omega) = S_{\tilde{x}\tilde{y}}^*(\omega)$ . Substituting (19)–(21) into (22)–(24) we obtain

$$S_x(\omega) = \frac{A^2}{4} \left( \frac{\cos^2 \psi}{\rho^2} + \rho^2 \sin^2 \psi \right) \times \left\{ \frac{1}{\alpha^2 + (\omega - \beta)^2} + \frac{1}{\alpha^2 + (\omega + \beta)^2} \right\}, \quad (25)$$

$$S_y(\omega) = \frac{A^2}{4} \left( \frac{\sin^2 \psi}{\rho^2} + \rho^2 \cos^2 \psi \right) \times \left\{ \frac{1}{\alpha^2 + (\omega - \beta)^2} + \frac{1}{\alpha^2 + (\omega + \beta)^2} \right\}, \quad (26)$$

$$\begin{aligned} S_{xy}(\omega) &= \frac{A^2}{4} \left( \frac{\cos \psi \sin \psi}{\rho^2} - \rho^2 \cos \psi \sin \psi \right) \times \\ &\times \left\{ \frac{1}{\alpha^2 + (\omega - \beta)^2} + \frac{1}{\alpha^2 + (\omega + \beta)^2} \right\} \\ &+ \frac{iA^2}{4} \left\{ \frac{1}{\alpha^2 + (\omega - \beta)^2} - \frac{1}{\alpha^2 + (\omega + \beta)^2} \right\}. \end{aligned} \quad (27)$$

We then convert back to complex using the relationships given in [8]

$$S_z(\omega) = S_x(\omega) + S_y(\omega) + 2\mathcal{I}\{S_{xy}(\omega)\}, \quad (28)$$

$$R_z(\omega) = S_x(\omega) - S_y(\omega) + 2i\mathcal{R}\{S_{xy}(\omega)\}. \quad (29)$$

Substituting (25)–(27) into (28)–(29) we obtain

$$\begin{aligned} S_z(\omega) &= \frac{A^2}{4} \left( \frac{1}{\rho^2} + \rho^2 \right) \\ &\times \left\{ \frac{1}{\alpha^2 + (\omega - \beta)^2} + \frac{1}{\alpha^2 + (\omega + \beta)^2} \right\} \\ &+ \frac{A^2}{2} \left\{ \frac{1}{\alpha^2 + (\omega - \beta)^2} - \frac{1}{\alpha^2 + (\omega + \beta)^2} \right\}, \\ R_z(\omega) &= \frac{A^2}{4} \left( \frac{1}{\rho^2} - \rho^2 \right) (\cos^2 \psi - \sin^2 \psi) \\ &\times \left\{ \frac{1}{\alpha^2 + (\omega - \beta)^2} + \frac{1}{\alpha^2 + (\omega + \beta)^2} \right\} \\ &+ \frac{iA^2}{2} \left( \frac{1}{\rho^2} - \rho^2 \right) \cos \psi \sin \psi \\ &\times \left\{ \frac{1}{\alpha^2 + (\omega - \beta)^2} + \frac{1}{\alpha^2 + (\omega + \beta)^2} \right\}, \end{aligned}$$

which simplify to the forms given in (9) and (10).

## REFERENCES

- [1] B. Picinbono and P. Chevalier, "Widely linear estimation with complex data," *IEEE transactions on Signal Processing*, vol. 43, no. 8, pp. 2030–2033, 1995.
- [2] J. Navarro-Moreno, "ARMA prediction of widely linear systems by using the innovations algorithm," *IEEE Transactions on Signal Processing*, vol. 56, no. 7, pp. 3061–3068, 2008.
- [3] A. M. Sykulski, S. C. Olhede, and J. M. Lilly, "A widely linear complex autoregressive process of order one," *IEEE Transactions on Signal Processing*, vol. 64, no. 23, pp. 6200–6210, 2016.
- [4] Y. Xia and D. P. Mandic, "Augmented performance bounds on strictly linear and widely linear estimators with complex data," *IEEE Transactions on Signal Processing*, vol. 66, no. 2, pp. 507–514, 2017.
- [5] P. Wen and J. Zhang, "Widely linear complex-valued diffusion subband adaptive filter algorithm," *IEEE Transactions on Signal and Information Processing over Networks*, vol. 5, no. 2, pp. 248–257, 2018.
- [6] S. Zhang, J. Zhang, W. X. Zheng, and H. C. So, "Widely-linear complex-valued estimated-input LMS algorithm for bias-compensated adaptive filtering with noisy measurements," *IEEE Transactions on Signal Processing*, 2019.
- [7] P. J. Schreier and L. L. Scharf, *Statistical signal processing of complex-valued data: the theory of improper and noncircular signals*. Cambridge University Press, 2010.
- [8] A. M. Sykulski, S. C. Olhede, J. M. Lilly, and J. J. Early, "Frequency-domain stochastic modeling of stationary bivariate or complex-valued signals," *IEEE Transactions on Signal Processing*, vol. 65, no. 12, pp. 3136–3151, 2017.
- [9] A. Oya, J. Navarro-Moreno, and J. C. Ruiz-Molina, "Widely linear simulation of continuous-time complex-valued random signals," *IEEE Signal Processing Letters*, vol. 18, no. 9, pp. 513–516, 2011.
- [10] A. M. Martínez-Rodríguez, J. Navarro-Moreno, R. M. Fernández-Alcalá, and J. C. Ruiz-Molina, "A general solution to the continuous-time estimation problem under widely linear processing," *EURASIP Journal on Advances in Signal Processing*, vol. 2011, no. 1, p. 119, 2011.
- [11] G. E. Uhlenbeck and L. S. Ornstein, "On the theory of the Brownian motion," *Physical Review*, vol. 36, no. 5, p. 823, 1930.
- [12] M. Arató, A. N. Kolmogorov, and Y. G. Sinai, "Evaluation of the parameters of a complex stationary Gauss-Markov process," *Doklady Akademii Nauk SSSR*, vol. 146, pp. 747–750, 1962.
- [13] M. Veneziani, A. Griffa, A. M. Reynolds, and A. J. Mariano, "Oceanic turbulence and stochastic models from subsurface Lagrangian data for the Northwest Atlantic Ocean," *Journal of Physical Oceanography*, vol. 34, no. 8, pp. 1884–1906, 2004.
- [14] A. M. Sykulski, S. C. Olhede, J. M. Lilly, and E. Danioux, "Lagrangian time series models for ocean surface drifter trajectories," *Journal of the Royal Statistical Society: Series C (Applied Statistics)*, vol. 65, no. 1, pp. 29–50, 2016.
- [15] J. Lilly and J.-C. Gascard, "Wavelet ridge diagnosis of time-varying elliptical signals with application to an oceanic eddy," *Nonlinear Processes in Geophysics*, vol. 13, no. 5, pp. 467–483, 2006.
- [16] Y. Barkin and J. Ferrandiz, "Elliptical Chandler pole motions of the Earth and Mars," in *EGU General Assembly Conference Abstracts*, vol. 12, 2010, p. 2936.
- [17] P. Vatiwutipong and N. Phewchean, "Alternative way to derive the distribution of the multivariate Ornstein–Uhlenbeck process," *Advances in Difference Equations*, vol. 2019, no. 1, pp. 1–7, 2019.
- [18] P. Brockwell, "Continuous-time ARMA processes," *Handbook of statistics*, vol. 19, pp. 249–276, 2001.
- [19] A. M. Sykulski and D. B. Percival, "Exact simulation of noncircular or improper complex-valued stationary Gaussian processes using circulant embedding," in *2016 IEEE 26th International Workshop on Machine Learning for Signal Processing (MLSP)*. IEEE, 2016, pp. 1–6.
- [20] P. M. Robinson *et al.*, "Gaussian semiparametric estimation of long range dependence," *The Annals of statistics*, vol. 23, no. 5, pp. 1630–1661, 1995.
- [21] A. M. Sykulski, S. C. Olhede, A. P. Guillaumin, J. M. Lilly, and J. J. Early, "The debiased Whittle likelihood," *Biometrika*, vol. 106, no. 2, pp. 251–266, 2019.
- [22] D. R. Brillinger, "An empirical investigation of the Chandler wobble and two proposed excitation processes," *Bulletin of the International Statistical Institute*, vol. 45, no. 3, pp. 413–434, 1973.
- [23] J. Vondrák, C. Ron, and Y. Chapanov, "New determination of period and quality factor of Chandler wobble, considering geophysical excitations," *Advances in Space Research*, vol. 59, no. 5, pp. 1395–1407, 2017.
- [24] J. Höpfner, "Chandler and annual wobbles based on space-geodetic measurements," *Journal of Geodynamics*, vol. 36, no. 3, pp. 369–381, 2003.
- [25] J. M. Lilly and S. C. Olhede, "Bivariate instantaneous frequency and bandwidth," *IEEE Transactions on Signal Processing*, vol. 58, no. 2, pp. 591–603, 2009.
- [26] J. M. Lilly, "Modulated oscillations in three dimensions," *IEEE Transactions on Signal Processing*, vol. 59, no. 12, pp. 5930–5943, 2011.
- [27] J. M. Lilly and S. C. Olhede, "Analysis of modulated multivariate oscillations," *IEEE Transactions on Signal Processing*, vol. 60, no. 2, pp. 600–612, 2011.
- [28] M. Barigozzi, H. Cho, and P. Fryzlewicz, "Simultaneous multiple change-point and factor analysis for high-dimensional time series," *Journal of Econometrics*, vol. 206, no. 1, pp. 187–225, 2018.
- [29] J. Chang, B. Guo, Q. Yao *et al.*, "Principal component analysis for second-order stationary vector time series," *The Annals of Statistics*, vol. 46, no. 5, pp. 2094–2124, 2018.
- [30] Z. Che, S. Purushotham, K. Cho, D. Sontag, and Y. Liu, "Recurrent neural networks for multivariate time series with missing values," *Scientific reports*, vol. 8, no. 1, p. 6085, 2018.
- [31] D. Hallac, S. Vae, S. Boyd, and J. Leskovec, "Toeplitz inverse covariance-based clustering of multivariate time series data," in *Proceedings of the 23rd ACM SIGKDD International Conference on Knowledge Discovery and Data Mining*. ACM, 2017, pp. 215–223.
- [32] F. H. Nieto, D. Pena, and D. Saboyá, "Common seasonality in multivariate time series," *Statistica Sinica*, pp. 1389–1410, 2016.
- [33] S. Olhede and A. Walden, "Local directional denoising," *IEEE transactions on signal processing*, vol. 53, no. 12, pp. 4725–4730, 2005.
- [34] F. Lindgren, H. Rue, and J. Lindström, "An explicit link between Gaussian fields and Gaussian Markov random fields: the stochastic partial differential equation approach," *Journal of the Royal Statistical Society: Series B (Statistical Methodology)*, vol. 73, no. 4, pp. 423–498, 2011.
- [35] A. Walden, "Rotary components, random ellipses and polarization: a statistical perspective," *Philosophical Transactions of the Royal Society A: Mathematical, Physical and Engineering Sciences*, vol. 371, no. 1984, p. 20110554, 2013.
- [36] T. Van Hoolst, V. Dehant, and P. Defraigne, "Chandler wobble and free core nutation for Mars," *Planetary and Space Science*, vol. 48, no. 12–14, pp. 1145–1151, 2000.